Geometric constraints for the design of diffusing-wave spectroscopy experiments

P. D. Kaplan, Ming Hsii Kao, A. G. Yodh, and David J. Pine

Diffusing-wave spectroscopy (DWS) experiments require the choice of suitable sample geometry. We study sample geometries for transmission experiments by performing DWS measurements on a variable thickness cell. The data reveal that DWS works well, giving consistent answers to within 5% when the cell is more than 10 random walk step lengths thick, and that the input geometry is less significant when sample cells are immersed in water than when they are surrounded by air. Further, we see that the applicability of the diffusion approximation depends on the anisotropy of individual scattering events.

The development of diffusing-wave spectroscopy[1–3] (DWS) has made it possible to use diffuse light to study the motion of particles in opaque suspensions. In this paper, we present a few simple DWS experiments designed to provide clear answers to some basic design questions about DWS transmission experiments. In particular, we consider the importance of diffuse reflection, input spot size, and sample thickness on the final results of DWS measurements. We include several appendixes that address technical points of DWS that should be useful to practitioners.

In a DWS experiment, a laser beam strikes a slab of scattering material, and the temporal autocorrelation function of a small fraction of the light that passes through the slab is measured. The transport of light through the slab is treated as a diffusive process that can be described by a single parameter, the photon diffusion coefficient D_γ. In this paper we discuss design issues such as the minimum slab thickness for which the diffusion approximation is good, the significance of the materials that contain the slab, and the impact of the input spot size on final DWS results. Previous work on the breakdown of the photon diffusion approximation[4] measured the temporal spreading of a short pulse of light through a slab. This does not directly tell us where DWS will fail, since DWS relies on additional assumptions about temporal correlations that are not needed in the photon diffusion approximation. Previous work[4] on the breakdown of the diffusion approximation also ignored external reflections and the importance of input spot size. Finally, we have tested the significance of scattering anisotropy on the applicability of DWS, a subject that to our knowledge has not been experimentally addressed.

There is a rich literature about the problem of photon transport in turbid media (see, for example, Refs. 5–7). In DWS the diffusion approximation is used to describe photon transport. In this approximation, photons are treated as random walkers, with random walk step length l^* and a resultant diffusion coefficient $D_\gamma = vl^*/3$, where v is the speed of light in the suspension. The diffusion approximation is valid for calculating transport only over distances larger than several l^*. When scattering is not isotropic, which is the case for particle sizes close to and larger than the photon wavelength, the random walk step length is larger than the photon mean free path length l. For optically thin samples, including samples that scatter once, l is the critical parameter, while for optically thick samples, l^* is the critical parameter. These lengths are connected by the expression[8]

$$\frac{l^*}{l} = \frac{2k_0^2}{\langle q^2 \rangle}, \tag{1}$$

where k_0 is the photon wave vector in the solvent and $\langle q^2 \rangle$ represents the average square scattering vector for a typical scattering event experienced by the photon in the medium.[8] We expect that when the diffusion approximation breaks down, we will see different behavior for samples with different values of l. Understanding data from thin samples requires

P. D. Kaplan, M. H. Kao, and A. G. Yodh are with the Department of Physics, University of Pennsylvania, Philadelphia, Pennsylvania 19104. D. J. Pine is with Exxon Research and Engineering Co., Route 22E, Annandale, New Jersey 08801.

Received 25 January 1993.
0003-6935/93/213828-09$06.00/0.

alternatives to the diffusion approximation[9] that are not considered here.

1. Experiment

Our multiple-scattering apparatus, Fig. 1, can be used for DWS or for measuring the static transmission coefficient of a sample. The apparatus consisted of an Ar^+ ion laser operating at a wavelength of 514.5 nm, a spatial filter, and collimating optics that produced a Gaussian beam with a FWHM of 2 cm; the central 2 cm of the beam were allowed to strike the sample. A single speckle of light transmitted through the sample was selected by two pinholes. To determine the transmission, the ratio of transmitted to reflected intensities was measured and compared with a standard sample for calibration. For the dynamic measurements, in order to obtain fast correlations with minimal effects from afterpulsing in the photomultiplier tubes, we split the output speckle between two photomultiplier tubes and measured their cross correlation. The measured cross correlation was related to the field correlation function $g_1(\tau)$, discussed below, through the Siegert relationship:

$$\frac{\langle I(0)I(\tau)\rangle}{\langle I(0)\rangle^2} = 1 + \beta_G|g_1(\tau)|^2, \qquad (2)$$

where β_G is an experimental parameter that depends on the size and separation of the pinholes; it was 0.18 in our apparatus.[10] When we fit intensity correlation functions, β_G was always a free parameter. An example of a measured and fit correlation function is found in Fig. 2.

To reduce the systematic effects that arise in sample preparation, we varied the optical thickness by changing the length of the cell rather than by changing the sample's volume fraction. The variable path-length cell was constructed of stainless steel with teflon seals and quartz windows. The importance of transverse boundaries is discussed in Section 5. The partially reflecting steel boundary is unimportant for the relatively thin settings used in this experiment. The cell was a cylinder with a 2-cm diameter and a thickness that was variable from 70 μm to 1 cm; in this paper, the cell thickness is reported in units of the photon random walk step length l^* in the samples. This number can be found for each sample in Table 1. There is an uncertainty of a few percent in the calculated value of l^*, and hence we never know the cell thickness in units of l^* to better than 2–3%. The cell was equipped with a reservoir that held several milliliters of sample when the cell thickness was reduced. The cell's path length was calibrated against a fixed thickness cuvette in a spectrophotometer by the use of a green dye (McCormick's food coloring) with two absorption peaks. From this calibration we determined the cell thickness to within 5 μm for each measurement reported here.

Samples were prepared with polystyrene spheres with diameters of 205 and 460 nm at a volume fraction ϕ of ~ 0.017. A small amount (0.1% by weight) of sodium dodecyl sulfate, an adsorbing surfactant, was added to ensure long-term stability. The salt concentration was maintained at high enough

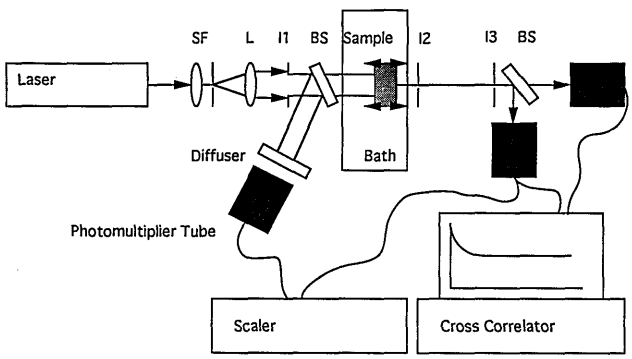

Fig. 1. Experimental apparatus. The beam from a cw Ar^+ ion laser is expanded by spatial filter SF and collimated with lens L. The flat, central 2 cm of this beam passes through iris I1 and then illuminates a slab of scattering particles that may or may not be immersed in water. A single speckle of transmitted light is selected by two pinholes (I2 and I3) and split (by beam splitter BS) between two photomultiplier tubes. The intensity cross-correlation function of the two tubes is monitored by a commercial correlator. To measure transmission coefficients, the laser power is sampled by a beam splitter placed in front of the sample so that the ratio of transmitted intensity to laser intensity can be monitored.

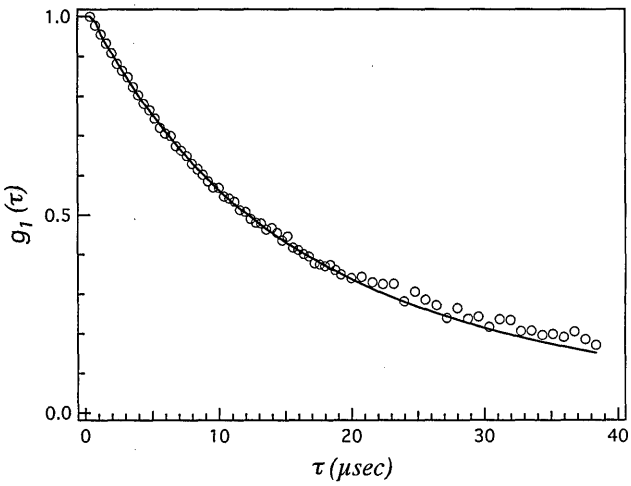

Fig. 2. Normalized correlation function $g_1(\tau)$ obtained from a ϕ = 0.0443 sample of 460-nm-diameter spheres, with L = 750 μm, l^* = 51 μm, and T = 25 °C. The solid curve is the best fit, from the procedures described in the appendixes, with a reflection coefficient of 0.02.

Table 1. Samples Studied[a]

Diameter (mm)	ϕ	l^* (Mie theory) (μm)	l^*/l
205	0.01798 ± 0.00013	120 ± 2	8
460	0.01665 ± 0.00013	137 ± 2	26

[a]The uncertainty in l^* is dominated by an uncertainty of ±%1 in the index of refraction of polystyrene. The ratio of the random walk step length l^* to the mean free path l is a measure of the anisotropy of single-scattering events.

levels so that the screening length was less than 5 nm. Both samples had approximately the same value for l^*, but because the particle diameters varied, the ratio of the random walk step length l^* to the distance between scattering events l was different. A detailed description of the samples appears in Table 1.

The horizontal axes of many graphs in this paper are in units of optical thickness or L/l^*. We use the value of l^* calculated from the Mie scattering theory, assuming that the index of refraction of the particles is 1.583 (see Ref. 11) at $\lambda = 514.5$ nm and that the index of water is 1.336. Note that 1% errors in the indices of refraction will change the calculated l^* by a few percent. The uncertainties reported in Table 1 reflect both the small uncertainty in ϕ and an uncertainty of 1 part in 100 in the ratio $n_{H_2O}/n_{polystyrene}$.

2. Static Transmission

The static transmission coefficient can be calculated within the photon diffusion approximation. The transmission T through a slab of infinite transverse extent and thickness L is proportional to the photon random walk step length l^* (see appendix A):

$$T = (5/3)(l^*/L)[1 + (4/3)(l^*/L)]^{-1}. \qquad (3)$$

If absorption length l_a is of the order of L^2/l^* or less, this result is modified by a factor of $\beta/\sinh(\beta)$, where β is $(3L^2/l^*l_a)^{1/2}$.[12] In the present work we ignore absorption, as l_a is of the order of a few meters, and average pathlengths, which are of the order of L^2/l^*, are always less than 15 cm. The cell's optical transmission was measured by comparing the intensity transmitted into the receiving photomultiplier tubes with the intensity collected from the first beam splitter in Fig. 1. The resulting ratio drifts when the laser's spatial mode shifts during the course of an experiment. To normalize for that drift, the transmission of a standard cell was measured repeatedly. Thus we are able to measure only the ratio of the transmission of the sample cell to a standard cell. Repeated measurements at the same thickness indicate that transmission measurements obtained in this apparatus fluctuate by ~4%. This systematic uncertainty dominates the error bars in Fig. 3.

In Fig. 3, we see the value of l^* inferred from static transmission measurements. The measured transmission coefficient is converted to an apparent value of l^*/L by the complete version of Eq. (3) found in appendix A [Eq. (A11)]. The resulting numbers are normalized by the average of all measurements with $L/l^* > 10$. We see in Fig. 3 that for samples thicker than $5l^*$ the diffusion approximation appears to correctly predict the total transmission coefficient. We also note, however, that for the sample with more isotropic scattering (205-nm spheres) Eq. (3) breaks down for values of L/l^* less than 5 or 6, while the cell with more anisotropic scattering (460-nm spheres) works well down to L/l^* of ~2. The factor of 3 difference is strikingly similar to the factor of 3 difference in the distance between scattering events

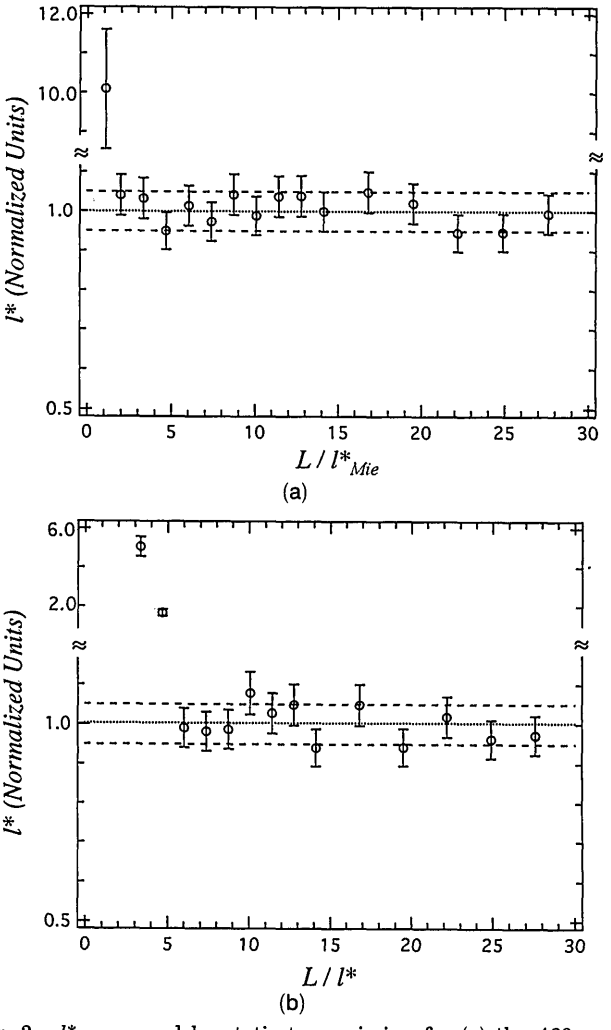

Fig. 3. l^* measured by static transmission for (a) the 460-nm system in water, (b) the 205-nm system in water. The units are normalized to the average measured l^* for $L/l^* > 10$.

(Table 1). This suggests that the critical measure of the applicability of the diffusion approximation might be the cell thickness measured in units of the distance between scattering events (L/l) rather than in units of the random walk step length (L/l^*).

3. Diffusing-Wave Spectroscopy

The theory of DWS makes the connection between temporal intensity fluctuations of the speckle field emerging from the sample and the dynamics of the particles in the sample. In this section, we present the basic result of DWS and highlight some of the assumptions commonly associated with DWS. This is neither an introduction to, nor a complete presentation of, DWS. For more detail, see Ref. 8.

In single-scattering experiments, all observed photons travel nearly the same distance to the detector, and the scattering angle is well known. In DWS, however, photon path lengths are typically distributed over several centimeters. The detected photons have scattered many times, through all possible angles. The photon random walk step length l^* is

the only parameter needed to describe diffusive transport. It is calculated from the photon mean free path by averaging over scattering angles: $l^*/l = 2k_0^2/\langle q^2\rangle$.

In the derivation of DWS, one first calculates the temporal field autocorrelation function for the case in which all photons travel the same distance through the sample:

$$g_1^{(s)}(\tau) = \frac{\langle E_{(s)}^*(0)E_{(s)}(\tau)\rangle}{\langle |E_{(s)}(0)|^2\rangle} = \exp[-2k_0^2\langle\Delta r^2(\tau)\rangle(s/l^*)/6], \quad (4)$$

where k_0 is the photon wave vector in the solvent, and $\langle\Delta r^2(\tau)\rangle$ is the mean squared displacement of a diffusing particle in time τ. The measured correlation function includes contributions from a distribution of path lengths, $P(s)$, and the result of the measurement is the weighted average

$$g_1(\tau) = \int_0^\infty P(s)\exp[-2k_0^2(s/l^*)D\tau]ds, \quad (5)$$

where $P(s)$ is the photon path-length probability distribution. In the presence of absorption, a factor of $\exp(-s/l_a)$ would be included in the integral, decreasing the contributions from long paths. This basic expression has been verified in several ways[8,13] for samples well into the diffusive regime.

Equation (5) can be evaluated exactly for the transmission of a plane wave through a slab of thickness L and infinite transverse extent:

$$g_1(\tau) = \left(\frac{L/l^* + 2\beta}{\alpha + \beta}\right) \times \frac{\sinh(\alpha x) + \beta x\cosh(\alpha x)}{(1 + \beta^2x^2)\sinh(xL/l^*) + 2\beta x\cosh(xL/l^*)}, \quad (6)$$

where $\beta = (2/3)(1 + R)/(1 - R)$, R is the diffuse reflection coefficient,[14] $x = k_0\langle\Delta r^2(\tau)\rangle^{1/2}$, and α is a parameter explained in appendix A that is roughly equal to 1. For simple diffusive motion, $\langle\Delta r^2(\tau)\rangle = 6D\tau$, where $D = k_BT/6\pi\eta a$ is the Einstein diffusion coefficient and a is the particle radius. Including absorption in this result is relatively straightforward following the methods of Ref. 8. We have used a more complex expression, given in Appendix C, which includes the hydrodynamic interactions between the particle and the surrounding fluid. If we had omitted these complications of hydrodynamics, our results would have changed by less than 3%. Hydrodynamic effects are most significant, however, at times that are comparable with the hydrodynamic time (Appendix C). In thicker samples, where photon path lengths are longer and the times probed by DWS are correspondingly shorter, the full hydrodynamic calculation becomes more important.

All expressions for $g_1(\tau)$ depend on both the optical parameter L/l^* and the particles' dynamics $\langle\Delta r^2(\tau)\rangle$. Each expression for $g_1(\tau)$ can thus be fit by assuming knowledge of one of these quantities and fitting to the other. In this experiment we know the particle dynamics well, and we study various approaches to the data by seeing how they affect the apparent value of l^*.

Determinations of l^* from dynamic data show the same trends as were observed by static transmission. In Fig. 4, we plot l^* as determined for cells immersed in water by fitting measured functions to the best valueof l^*. When L/l^* is less than 10 we begin to see larger variations in l^*. Comparing the data from the 460- and 205-nm systems shows that the point at which DWS fails depends on the anisotropy of the scattering form factor; the minimum cell thickness is closer to $4l^*$ for the 460-nm particles and $9l^*$ for the 205-nm particles. Apparently, the diffusion approximation is valid for transport over shorter distances in samples with more anisotropic scattering and hence more scattering events per l^*.

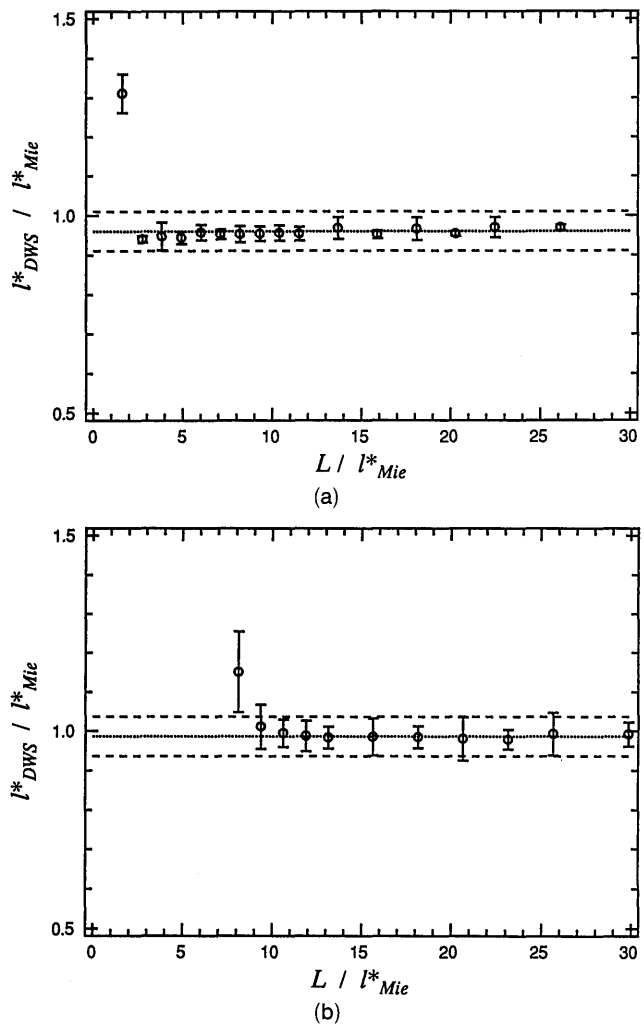

Fig. 4. l^* measured by fitting to $g_2(\tau)$. The cells containing (a) 460-nm particles and (b) 205-nm particles are submerged in a water bath.

4. Surface Reflectivity

Generally, DWS experiments have been analyzed by the use of a plane-wave input–point output geometry without diffuse reflection. In fact, the index of refraction of the cell walls is rarely matched to the solvent and, even worse, after moving from the sample to the cell wall, all photons traveling at sufficiently oblique angles will suffer total internal reflection and be returned to the sample. We estimate that the critical angle for a water–glass–air interface is 50°, while for water–glass–water there is no critical angle. The diffuse reflection coefficient can be calculated from an angular average over the Fresnel reflection coefficients[14] (see Appendix B).[5,15–21] We estimate that the diffuse reflection coeffcient in water is ~0.02, while the coefficient in air may be as large as 0.10. In our calculation, we include only a finite number of multiple reflections. The number of reflections included depends on the cell size (2 cm) and the cell wall thickness (2 mm). Without this truncation, the calculated reflection coefficient could be as much as three times larger. In order to see the effects of these boundary conditions, we performed measurements on the same system with the sample cell both in and out of water.

The DWS data in Fig. 5 reveal essentially the same results as the data in water (Fig. 4). Two determinations of l^* are plotted; one ignores reflectivity and the other assumes that R is 0.1. Ignoring reflectivity adds a small, but systematic, slope to the data for L/l^* less than 12.

Removing water from the bath surrounding the cell will change the diffuse surface reflectivity, which should change the absolute transmission (see appendix A). Removing the water also effectively changes our collection optics. This systematic change prevents us from directly comparing transmissions with

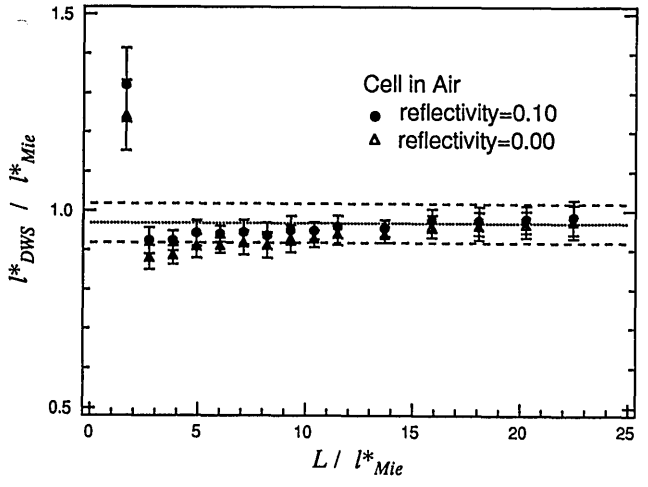

Fig. 5. l^* measured by fitting to $g_2(\tau)$ for the cell of 460-nm particles after the water was drained from the index-matching bath. This fit was done twice. The first time, the correct reflection coefficient was included (circles), and the data appear flat down to L/l^* of ~3. The second fits (triangles) were done without reflection, and a systematic slope is present for samples thinner than ~12l^*.

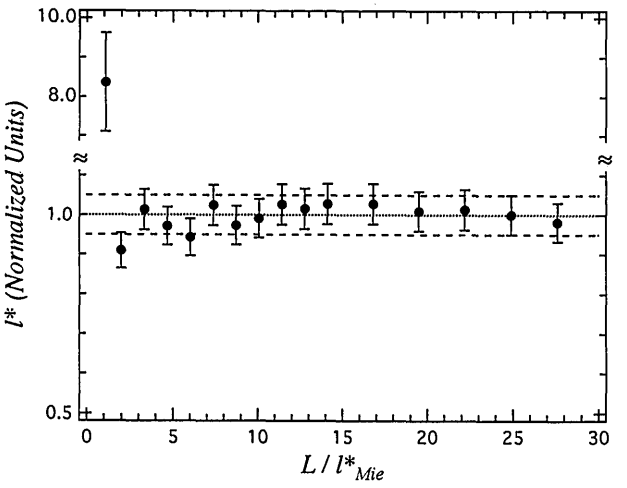

Fig. 6. Static transmission measured for the 460-nm particles after the water was drained from the index-matching bath.

and without water in the bath. We can demonstrate, however, that the trends are the same in both air and water for thick samples by comparing Figs. 3(a) and 6. The departure of T from the diffusive result still appears to occur for cells thinner than 4 or 5l^*.

5. Plane-Wave Approximation

All the results above use a path-length distribution $P(s)$ that is derived for the transmission of a plane wave through a slab of infinite transverse extent. In fact, our slabs and our laser beams are always finite. We have investigated this limitation in two ways. First, we tried using the full cylindrical solution to the diffusion equation for an input spot of finite size and Gaussian intensity profile,[22,23] rather than relying on the plane-wave approximation. This systematically changes our results by less than 3%.

Additional measurements were performed on 500-μm-thick cells containing 460-nm polystyrene spheres at a volume fraction of 0.044. With this sample, we varied the input spot size by aperturing a Gaussian

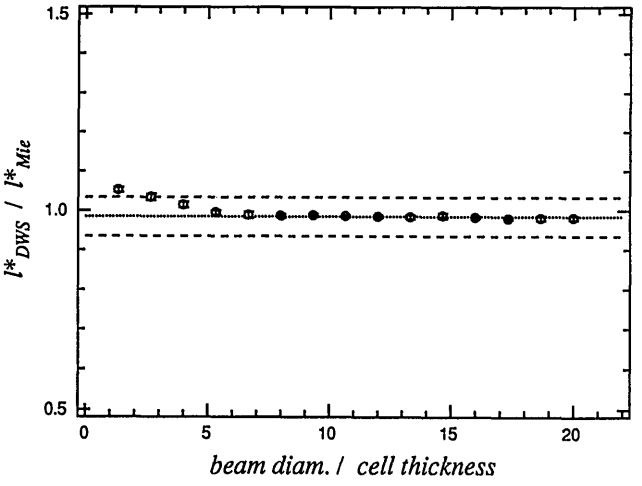

Fig. 7. l^* determined for various sizes of the input spot size. It appears that the plane-wave approximation works well for beam diameters larger than 5 times the cell thickness.

beam with a FWHM diameter of 2 cm, rather than by varying cell thickness L (see Fig. 7). This experiment was performed with cells placed in air and in water to see if diffuse reflection changes the applicability of the plane-wave approximation.

The surface reflectivity is relatively unimportant in this measurment. We see, however, that a beam diameter of at least 5 cell thicknesses is desirable when the plane-wave approximation is used.

6. Conclusions

We have tested the applicability of DWS in different experimental geometries. It appears that DWS works best for sample cells with $L/l^* > 10$ and for an input spot with a diameter greater than $5L$. The minimum cell thickness for DWS appears to be close to, but perhaps slightly larger than, the minimum cell thickness for which the diffusion approximation correctly calculates the total transmission coefficient. Further, we have demonstrated that the exact point at which both DWS and the diffusion approximation fail depends on the anisotropy of individual scattering events or perhaps simply on the raw number of collisions. The breakdown point can be as thin as $L/l^* > 3$. The utility of the diffusion approximation for relatively thin samples with large l^*/l is of great importance for systems with strongly anisotropic scattering, such as biological systems and systems of micrometer-sized and larger particles. Although the size and the effects of surface reflections can be estimated, we believe that it is simpler and more reliable to minimize them by submerging sample cells in an index-matching fluid such as water.

The actual breakdown point of the diffusion approximation depends on boundary conditions and scattering properties of individual samples. The breakdown also appears to be rather sudden, generally growing larger than 5% for changes of just 1 or 2 l^* in the sample thickness. As a practical matter, then, it is not desirable to work close to the limits set in this paper unless there is some certainty about l^* for a given sample.

Appendix A: Derivation of Transmission Coefficient

The total transmission coefficient for a slab calculated within the diffusion approximation without photon absorption is basically proportional to l^*/L.

$$T = \frac{5l^*}{3L}\left(1 + \frac{4l^*}{3L}\right)^{-1}. \tag{A1}$$

This appendix contains a simple derivation of this result. The transmission coefficient is independent of the profile of the input beam for a slab of infinite transverse extent. We choose to solve the simplest problem, the one-dimensional photon diffusion problem, and then use this solution to compute the flux at both faces. The transmission is then calculated by dividing the transmitted flux by the total flux. There are many other derivations of Eq. (A1).[5,15–21] Within the diffusion approximation in the absence of absorption, photon transport is described by the diffusion of photon energy density U:

$$\partial_t U = D_\gamma \nabla^2 U, \tag{A2}$$

where $D_\gamma = cl^*/3$ is the photon transport diffusion coefficient, and c is the speed of light in the scattering medium. We consider the steady-state, one-dimensional problem pictured in Fig. 8,

$$\partial_z{}^2 U = 0, \tag{A3}$$

which has straight lines as a solution. We further assume that the incident flux appears as a diffuse source at some distance αl^* inside the sample, $\alpha \approx 1$, e.g., $U(\alpha l^*) = 2U_0$. Now the solution is of the form

$$U = \begin{cases} A_l + B_l z & \text{for } z < \alpha l^* \\ A_r + B_r z & \text{for } z > \alpha l^* \end{cases}. \tag{A4}$$

To solve for the A and B coefficients we need the correct boundary conditions.

The boundary conditions require that the duffuse flux into the sample, at the boundary, be solely due to reflections. The net current **J**, given by Fick's law, can be considered as the sum of the currents in each direction[8,5]:

$$\mathbf{J} \cdot \hat{z} = J_+ - J_- = -D\hat{z} \cdot \nabla U. \tag{A5}$$

The current in each direction has an isotropic component[24]

$$J_\pm = \frac{Uc}{4} \mp \frac{D_\gamma}{2}\partial_z U. \tag{A6}$$

In terms of this current, the boundary conditions are

$$J_+(0) = RJ_-(0), \tag{A7}$$

$$J_-(L) = RJ_+(L), \tag{A8}$$

where R is the diffuse reflection coefficient. The final condition is that U has no discontinuity at $z =$

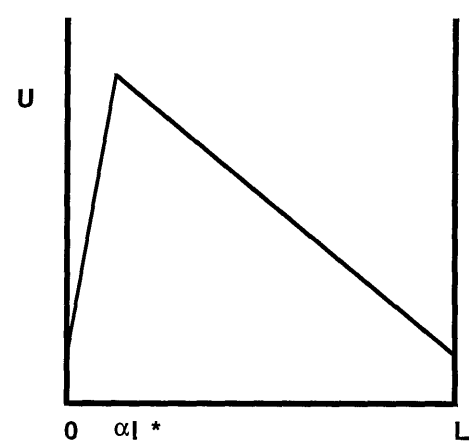

Fig. 8. Energy density U is displayed for the one-dimensional steady-state problem. From this solution to the diffusion equation, we derive the transmission coefficient of a slab of optical thickness L/l^* in appendix A.

αl^*. We now have three boundary conditions for the four coefficients. We arbitrarily set A_l to U_0 and find

$$U = U_0 \begin{cases} (1 + z/hl^*) & \text{for } z < \alpha l^* \\ \dfrac{1 + \alpha/h}{L + (h - \alpha)l^*}(L + hl^* - z) & \text{for } z > \alpha l^* \end{cases}, \tag{A9}$$

where $h = (2/3)(1 + R)/(1 - R)$. With this solution for the energy density, the transmission coefficient is readily obtained by the use of the transmitted and the backscattered fluxes.

Thus the total transmission is

$$T = \frac{J_+(L)}{J_+(L) + J_-(0)}, \tag{A10}$$

which is evaluated with Eq. (A6), giving

$$T = \left(\frac{l^*}{L}\right) \frac{\frac{2}{3}\left(\frac{1 + R}{1 - R}\right) + \alpha}{1 + \frac{4}{3}\left(\frac{1 + R}{1 - R}\right)\frac{l^*}{L}}. \tag{A11}$$

The prefactor of 5/3 in Eq. (A1) is obtained by setting R to 0 and α to 1. It depends on both the physical boundary conditions and on α, which is an artifact of this simple model. The denominator, however, depends on only the boundary conditions. We always measure the ratio of the transmission of different samples. This ratio is insensitive to the value of the prefactor in Eq. (A1).

Appendix B: Estimating Diffuse Reflection Coefficients

Boundary conditions have an impact on the details of all measurements involving diffuse light. In the previous appendix, the transmission coefficient was derived assuming knowledge of the reflection coefficient at the boundary. This reflection coefficient is also needed to calculate the correct distribution of photon path lengths through the sample and hence $g_1(\tau)$. For a single interface the calculation of the diffuse reflection coefficient by Zhu *et al.*[14] is quite good. For a double interface, such as that which occurs when the sample is contained in a cell whose walls have finite thickness, the calculation is harder. In this appendix we present our estimate of this real reflection coefficient.

The estimate involves multiple reflections and finite cell size. In addition to the diffuse reflection coefficient between a multiple-scattering sample and a nonscattering external medium $R_{12}(\theta)$,[14] we consider light that propagates to the second boundary and is reflected back into the sample, increasing the reflectivity by $T_{12}(\theta_1)R_{23}(\theta_2)T_{12}(\theta_2)$. In this section, θ_1 is the angle of incidence for light moving from the diffuse medium to the cell wall, and θ_2 is the angle at which light propagates in the cell wall (see Fig. 9). Snell's law is used to calculate $\theta_2(\theta_1)$. We need to include multiple reflections, but only a limited number of multiple reflections. At each reflection, a photon propagates $2d \tan(\theta_2)$ along the sample's surface. We choose to ignore multiple reflections that require that the photon be translated by more than half of the cell diameter D. That is, the number of reflections included in the calculation N_m is the smallest integer less than $D/4d \tan(\theta_2)$. The total reflection coefficient is

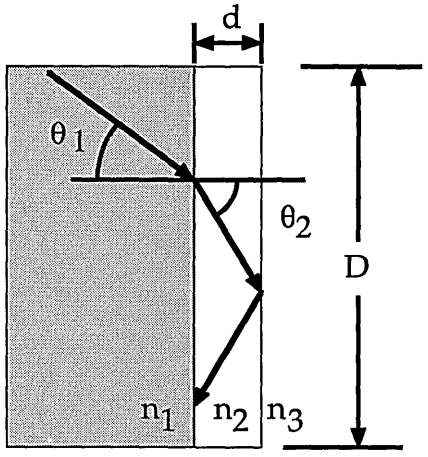

Fig. 9. Light leaving the cell of diameter D at an angle of θ_1 travels in the cell wall of thickness d at an angle θ_2, which is calculated by Snell's law. For θ_2 greater than the angle for total internal reflection, all light will be either reflected or carried along the cell wall to its edge. The total reflection coefficient can be greatly reduced by submerging the cell in water, which increases the angle of total internal reflection.

$$R(\theta) = R_{12}(\theta_1) + T_{12}(\theta_1)R_{23}(\theta_2)T_{21}(\theta_2) \times \sum_{j=0}^{j=N_m(\theta_2)} [R_{21}(\theta_2)R_{23}(\theta_2)]^j \tag{B1}$$

$$= R_{12}(\theta_1) + T_{12}(\theta_1)R_{23}(\theta_2)T_{21}(\theta_2) \times \frac{1 - [R_{21}(\theta_2)R_{23}(\theta_2)]^{N_m(\theta_2)}}{1 - R_{21}(\theta_2)R_{23}(\theta_2)}, \tag{B2}$$

where the R's and T's are polarization-averaged Fresnel reflection and transmission coefficients, respectively. The final reflection coefficient R is obtained from $R(\theta)$ in Eq. (B2) following the technique described in Ref. 14. The correct number of reflections to include in the sum is probably different at the center and the edge of the cell, a factor we have not considered. We emphasize that this is an approximate calculation that can be affected by factors such as our estimate of the relevant number of reflections N_m.

Appendix C: Short-Time Particle Motion

Recent work on short-time particle hydrodynamics emphasizes the fact that in many DWS experiments, the rms displacement of the particle $\langle \Delta r^2(\tau) \rangle$ is not well approximated by the familiar long-time result $\langle \Delta r^2(\tau) \rangle = 6D\tau$.[25,26] The hydrodynamic time scale, the time it takes for vorticity to traverse the particle's

diameter, is $\tau_\nu = \rho a^2/\eta$ is 55 ns for a 460-μm particle. Diffusive motion is not well established for as many as 100 τ_ν's. Decay times for a sample of reasonable optical thickness are often several hundred nanoseconds, which is of the order of the time it takes for nondiffusive hydrodynamic effects to decay. A full hydrodynamic treatment for a single suspended Brownian particle has been given by Hinch,[27] and yields a much more complex form of $\langle \Delta r^2(\tau) \rangle$:

$$\langle \Delta r^2(\tau) \rangle = 6D\left\{\tau - 2\left(\frac{\tau_\nu \tau}{\pi}\right)^{1/2} + \frac{2}{9}\tau_\nu\left(4 - \frac{\rho'}{\rho}\right) + \frac{3}{\left[\tau_\nu\left(5 - 8\frac{\rho'}{\rho}\right)\right]^{1/2}}\left[\frac{1}{a_+^{\,3}}\exp(a_+^{\,2}\tau) \times \operatorname{erfc}(a_+\sqrt{\tau}) - \frac{1}{a_-^{\,3}}\exp(a_-^{\,2}\tau)\operatorname{erfc}(a_-\sqrt{\tau})\right]\right\}, \quad \text{(C1)}$$

where

$$a_\pm = \frac{3}{2}\,\frac{3 \pm \left(5 - 8\frac{\rho'}{\rho}\right)^{1/2}}{\sqrt{\tau_\nu}\left(1 + 2\frac{\rho'}{\rho}\right)}, \quad \text{(C2)}$$

and ρ' and ρ are the densities of the particle and fluid, respectively. Note that, in general, the $a_\pm$ are complex and the two terms involving them are complex conjugates of each other. As a practical point, we remark that the usual power series expansions of the complementary error function work well with complex arguments. At high particle concentrations, interactions between particles become important and $g_1(\tau)$ wil contain contributions from collective density fluctuations, particularly if the mean interparticle distance is less than the wavelength of light. In this case, the quantity $\langle \Delta r^2(\tau) \rangle$ must be replaced by

$$\frac{\langle \Delta r^2(\tau) \rangle + [A(q, \tau)]}{[S(q)]}, \quad \text{(C3)}$$

where $S(q)$ is the structure factor of the suspension, and $A(q, \tau) = N^{-1}\,\Sigma_{i \neq j}^{N}\,\langle \Delta \mathbf{r}_i(\tau) \cdot \Delta \mathbf{r}_j(\tau) \exp\{i\mathbf{q} \cdot [\mathbf{r}_i(0) - \mathbf{r}_j(0)]\}\rangle$ is a time- and q-dependent factor that accounts for the correlated motions between particles.[28] The square brackets denote the q average, $[X] = \int_0^{2k_0a} X(q)F(q)q^3\mathrm{d}q / \int_0^{2k_0a} F(q)q^3\mathrm{d}q$, where $F(q)$ is the particle form factor. We have no way to evaluate the expression for $A(q, \tau)$ and choose instead to ignore it. An estimate of $[A(q, \tau)]$ may be made by calculating $[A(q, \infty)]$.[29] In the low concentration systems used in this study, the effect of ignoring $[A(q, \infty)]$ is less than 1%.

Ignoring the effects discussed in this appendix would have changed the values of l^* inferred by this paper by less than 3%. At higher volume fractions, these effects are more pronounced.

We gratefully acknowledge discussions with C. P. Gonatas and A. Lisyansky. This work was supported by the National Science Foundation through grant DMR-9003687. A. G. Yodh acknowledges partial support from the National Science Foundation through the Presidential Young Investigator program and from the Alfred P. Sloan Foundation.

References

1. G. Maret and P. E. Wolf, "Multiple light scattering from disordered media. The effect of Brownian motion of scatterers," Z. Phys. B **65,** 409–413 (1987).
2. M. J. Stephen, "Temporal fluctuations in wave propagation in random media," Phys. Rev. B **37,** 1–5 (1988).
3. D. J. Pine, D. A. Weitz, P. M. Chaikin, and E. Herbolzheimer, "Diffusing-wave spectroscopy," Phys. Rev. Lett. **60,** 1134–1137 (1988).
4. K. M. Yoo, Feng Liu, and R. R. Alfano, "When does the diffusion approximation fail to describe photon transport in random media?" Phys. Rev. Lett. **64,** 2647–2650 (1990); errata **65,** 2120–2121 (1992).
5. A. Ishimaru, *Wave Propagation and Scattering in Random Media* (Academic, New York, 1978).
6. C. F. Bohren and D. R. Huffman, *Absorption and Scattering of Light by Small Particles* (Wiley, New York, 1983).
7. C. F. Bohren, *Clouds in a Glass of Beer, Simple Experiments in Atmospheric Physics* (Wiley, New York, 1987).
8. D. J. Pine, D. A. Weitz, J. X. Zhu, and E. Herbolzheimer, "Diffusing-wave spectroscopy, dynamic light scattering in the multiple scattering limit," J. Phys. (Paris) **51,** 2101–2127 (1990).
9. B. J. Ackerson, R. L. Dougherty, N. M. Reguigui, and U. Nobbman, "Correlation transfer: application of radiative transfer solution methods to photon correlation problems," J. Thermophys. Heat Transfer **6,** 577–588 (1992).
10. E. Jakeman, C. J. Oliver, and E. R. Pike, "The effects of spatial coherence on intensity fluctuation distributions of Gaussian light," J. Phys. A **3,** L45–L48 (1970).
11. M. J. Devon and A. Rudin, "A simple technique for measuring the refractive index of polymer latexes at various wavelengths," J. Appl. Polymer Sci. **34,** 469–476 (1987).
12. D. J. Durian, D. A. Weitz, and D. J. Pine, "Multiple light-scattering probes of foam structure and dynamics," Science **252,** 686–688 (1991).
13. A. G. Yodh, P. D. Kaplan, and D. J. Pine, "Pulsed diffusing-wave spectroscopy: High resolution through nonlinear optical gating," Phys. Rev. B **42,** 4744–4747 (1990).
14. J. X. Zhu, D. J. Pine, and D. A. Weitz, "Internal reflection of diffusive light in random media," Phys. Rev. A **44,** 3948–3959 (1991).
15. A. Lagendijk, R. Vreeker, and P. DeVries, "Influence of internal reflection on diffusive transport in strongly scattering media," Phys. Lett. A **136,** 81–88 (1989).
16. Th. M. Nieuwenhuizen, Van der Waals-Zeeman Laboratorium, Valckenierstraat 65, 1018 XE Amsterdam, The Netherlands, and J. M. Luck, Sérvice de Physique Théorique, Centre d'Etudes de Saclay, 91191 Gif-sur-Yvette Cedex, France (personal communication, 1993).
17. A. Z. Genack, N. Garcia, and W. Polkosnik, "Long-range intensity correlation and the approach to localization," Waves Random Media **3,** s57–s64 (1991).
18. L. Svaasand, R. Haskell, B. J. Tromberg, T. Tsay, and McAdams, "Properties of photon density waves at boundaries," in *Photon Migration and Imaging in Random Media and Tis-*

sues, R. R. Alfano and B. Chance, eds., Proc. Soc. Photo-Opt. Instrum. Eng. **1888** (to be published).
19. B. J. Tromberg, T. Tsay, R. Haskell, L. Svaasand, and A. Braniff, "Influence of boundaries on photon density waves in tissues," in *Photon Migration and Imaging in Random Media and Tissues,* R. R. Alfano and B. Chance, eds., Proc. Soc. Photo-Opt. Instrum. Eng. **1888** (to be published).
20. R. Aronson, Polytechnic University, Brooklyn, New York 11201 (personal communication, 1993).
21. C. P. Gonatas, M. Ishii, M. Miwa, J. Schotland, B. C. Chance, and J. Leigh, "Determination of optical mean free path from pulse propagation and backscattering," Phys. Rev. E (to be published).
22. H. S. Carslaw and J. Jaeger, *Conduction of Heat in Solids* (Oxford U. Press, New York, 1986).
23. D. A. Weitz and D. J. Pine, "Diffusing-wave spectroscopy," in *Dynamic Light Scattering,* W. Brown, ed. (Oxford U. Press, New York, 1993), Chap. 16.
24. S. Glasstone and M. C. Edlund, *The Elements of Nuclear Reactor Theory* (Van Nostrand, Princeton, N.J., 1952), Chap. 1.
25. M. H. Kao, A. G. Yodh, and D. J. Pine, "Observation of Brownian motion on the time scale of hydrodynamic interactions," Phys. Rev. Lett. **70,** 242–245 (1992).
26. D. A. Weitz, D. J. Pine, P. N. Pusey, and R. J. A. Tough, "Nondiffusive Brownian motion studied by diffusing-wave spectroscopy," Phys. Rev. Lett. **63,** 1747–1750 (1989).
27. E. J. Hinch, "Application of the Langevin equation to fluid suspensions," J. Fluid Mech. **72,** 499–511 (1975).
28. J. Zhu, "Diffusing-wave spectroscopy," Ph.D. dissertation (City University of New York, New York, N.Y., 1992).
29. C. W. J. Beenakker and P. Mazur, "Diffusion of spheres in a concentrated suspension II," Physica **126A,** 349–370 (1984).